Schwanke, AJ.; Pergher, S.; Díaz Morales, UM.; Corma Canós, A. (2017). The influence of swelling agents molecular dimensions on lamellar morphology of MWW-type zeolites active for fructose conversion. Microporous and Mesoporous Materials. 254:17-27. doi:10.1016/j.micromeso.2016.11.007

Journal of Materials Chemistry A

ARTICLE

Molecular dimensions influence of swelling agents on lamellar morphology of MWW-type zeolites active for fructose conversion

A. J. Schwanke[a], S. B. C. Pergher[a], U. Díaz[b], A. Corma[b]

Received 00th January 20xx,
Accepted 00th January 20xx

DOI: 10.1039/x0xx00000x

www.rsc.org/

A new route to obtain pillared, disordered or desilicated MWW-type zeolites was developed assisted by quaternary ammonium surfactants with different hydrocarbon tail size acting as swelling agents ($C_{12}TA^+$, $C_{16}TA^+$, $C_{18}TA^+$). Effect of surfactant concentration and swelling conditions were determinant to obtain MWW-type zeolites with different lamellar organization and spatial distribution of individual zeolitic layers. Specifically, soft swelling at 25 °C preserved layer structure instead of aggressive processes at 80 °C that favored desilication, damaging the layers structure in case of $C_{12}TA^+$ and $C_{16}TA^+$ and $C_{18}TA^+$. It was proved that surfactant size combining with swelling and pillaring procedure influenced on physico-chemical and morphological nature of MWW-type materials. The obtained derivative MWW zeolites with different morphology, order and acessibility levels were firstly evaluated by catalitic dehydration fructose to 5-hydroxymethylfurfural showing, superior activity compared to commercial zeolite catalyst.

Introduction

Zeolites are microporous crystalline aluminosilicates composed of tetrahedral bonds TO_4 (T= Si or Al usually) coordinated by oxygen atoms. The different spatial organization between these tetrahedral units and their relationships generate different topologies of ordered porous structures with shape selectivity that play an important role in adsorption processes, ion exchange, separation, and catalysis.[1,2,3] However, the accessibility in the microporous range (usually, with pore sizes until 1 nm) imposes restriction for larger molecules that cannot access towards internal active sites, decreasing catalytic efficiency and imposing significant diffusional limitations.[4,5]

In contrast, zeolites with a hierarchical pore system have received growing attention in recent times.[4,6,7,8] The strategy based on generating secondary mesoporosity regions in zeolites emerges as a way to facilitate molecular diffusion and increase the variety of reagents capable to achieve and react with internal active sites.[6] Among the strategies "bottom-up" to hierarchy zeolites, pillaring process is able to separate individual layers of two-dimensional (2D) zeolitic precursors. This procedure creates mesoporous regions by inserting organic or inorganic species as pillars, located in the interlayer space, together with intrinsic microporosity present in the zeolitic layers.[9, 10] Considering the best examples in the state-of-art of successful hierarchical pillared zeolites, we found MCM-36 (MWW topology), ITQ-36 (FER topology) and recently, nanosheet pillared and self-pillared MFI-type zeolites.[11,12,13,14]

The MWW topology until now, offers the major versatility in zeolite modifications.[15] Specifically, for MCM-36, pillarization procedure is carried out after the swelling of MWW precursors with long chain surfactants. Normally, swelling procedures in aggressive conditions (high temperatures, 90 °C) were gently replace by mild conditions (ambient temperature) and successive washing cycles with intention of preserving the structure of individual layers. This modification facilitated the preparation of more stable and efficient catalysts, avoiding the partial silica dissolution and the preservation of the lamellar organization without the formation of undesirable mesoporous phase competitors.[16,17,18]. On the other hand, a recent study report that mild conditions could affect the swelling efficiency in MWW precursors with high Al content (Si/Al=~15) and varies depending on the type of cation-hydroxide used to generate high

[a] Universidade Federal do Rio Grande do Norte, Laboratório de Peneiras Moleculares, CEP: 59078-970, Natal, RN, Brazil
[b] Instituto de Tecnología Química, Universidad Politécnica de Valencia (UPV-CSIC) Av. de los Naranjos, s/n 46022, Valencia, Spain

† Electronic supplementary information (ESI) available: XRD of previous swelling materials with different surfactants (S1) Molecular dimensions of surfactants used to swelling (S2), pHs of swelling media (S3), loss mass values of swelling samples (S4), XRD of 18-A-10 calcined (S5), SEM of 18-A-10-P (S6) TEM of 16-A-10-P (S7), TEM of desilicated 12-A-10-P (S8), TEM of C, 18-S-10-P and 18-A-10-P (S9), BAS and LAS numbers of MWW-derivated materials (S10), rates of HMF production (S11), DTG for MWW-type materials after reaction of fructose conversion (S12).

pH in swelling treatment.[19] According to Roth et al,[15] the swelling step is historically the most difficult and critical step for modifying precursors. Moreover, the effect of swelling with different swelling agents has being widespread to other zeolite precursors as ICP-1 based on germanosilicate and offer diversity to create more open zeolites structures showing that in swelling and pillaring, tiny details determine everything.[20,21] Recently, new strategies for swelling/pillaring MWW-type materials, using dual-template agents and obtaining disordered zeolitic structures, have been reported.[22,23] However, the control of size galleries by surfactant size assisted method and pillaring process still need to be deeply explored.[15]

This work aims to evaluate the influence of long chain surfactants used as swelling agents, which exhibit different molecular dimensions, on pillared MWW-type zeolites through soft and aggressive swelling conditions. The obtained MWW-type zeolites with different physico-chemical nature, morphology and lamellar order were firstly evaluated by catalytic dehydration fructose to 5-hydroxymethylfurfural (5-HMF), being this an important reaction of conversion biomass to produce sustainable fuels.

Experimental

MCM-22 precursor synthesis: Synthesis of precursor (P) was done similarly to literature.[24] Thus, 0.37 g of NaOH (Sigma Aldrich) and 0.37 g of $NaAl_2O_3$ (Riedel-de-Haën), were dissolved in 81.18 g of distillated water. In a next step 4.98 g of hexamethyleneimine (HMI, Sigma Aldrich) and 6 g of fumed silica (Aerosil 200, Degussa) were added to the mixture. The resulting slurry with Si/Al ratio=~25 was stirred for 2 h and hydrothermally treated in PTFE-lined stainless-steel autoclave with rotation (60 rpm) at 135 °C for 7 days. After the aging period, the autoclave was quenched and the MCM-22 precursor filtered, washed with distilled water and dried overnight at 60°C. After calcination (580 °C for 12 h), resulting 3D-MCM-22 zeolite denoted (C).

Swelling precursor: Typically, 9.0 g of aqueous slurry of MCM-22(P) (20 wt% solids) was mixed with 35.0 g of an aqueous solution of 29 wt% $C_{18}TA^+Br/OH^-$, $C_{16}TA^+Br/OH^-$ or $C_{12}TA^+Br/OH^-$ (50, 51 and 53% ionic exchange, respectively). 11.0 g of an aqueous solution of 40 wt% TPA^+Br/OH^- (45% ionic exchange) was added, and the resultant slurry treated at 80°C (aggressive swelling) or 25°C (soft swelling) for 18 h. In Figure S1 it is shown the previous experiments that succeeded the choice of this surfactant mixture. Swollen materials were washed with distilled water by successive centrifugation cycles (12000 rpm) up to ten times and dried at 60°C for overnight. Aggressive or soft swelling treatments were denoted “A” and “S”, respectively, followed by “x” as number of washing cycles.

Pillaring: Swollen materials were added in tetraethyl orthosilicate (TEOS, 98%, Aldrich), 1:5 wt/wt, at 80°C for 24 in vigorous stirring under nitrogen atmosphere.[16] Due to successive centrifugation cycles that decrease the pH of the solution, each material was hydrolyzed with water (pH=9, controlled with NaOH) to ensure to complete hydrolysis of TEOS at 40°C for 12 hours and dried at 60°C for overnight. Calcination was done in tubular Pyrex reactor up to 550 °C with heating rate of 3 °C min^{-1} under nitrogen flow, followed by 8 hours under oxygen flow. All materials were converted to acidic form through three consecutive ion exchanges of 1 g of zeolite in 50 mL of 0.1 mol L^{-1} NH_4NO_3 (Aldrich) solution at ambient temperature for 3 h, and subsequent calcination at 500°C (heating rate of 5 °C min^{-1}) for 2 h under air atmosphere.

Catalytic tests: *Conversion of fructose to 5-hydroxymethylfurfural (5-HMF).* 218 mg of fructose and 18 mg of zeolite catalyst were added into a 10 mL Pyrex reactor, containing 8.0 g of dimethyl sulfoxide (DMSO). The formed mixture was stirred in an oil bath at 120 °C for 3h. The products, after fructose dehydration, were sampled at intervals and analyzed using HPLC. Fructose conversion (1), yield (2) and selectivity (3) of 5-HMF were calculated following the next equations: Conversion: $\frac{(C_{fructose})_0-(C_{fructose})_t}{(C_{fructose})_0} x\ 100\%$ (1)

Yield: $\frac{(C_{5-HMF})_t}{(C_{fructose})_0} x\ 100\%$ (2)

Selectivity: $\frac{(C_{5-HMF})_t}{(C_{fructose})_t} x\ 100\%$ (3)

Characterization: Powder X-ray diffraction (XRD) patterns were collected on a Philips X’Pert diffractometer equipped with a graphite monochromator, operating at 40 kV and 45 mA, using nickel-filtered CuKα radiation (λ = 0.1542 nm). Nitrogen adsorption isotherms at -196 °C were measured with a Micromeritics ASAP 2010 manometric adsorption analyzer. Before the measurements, the samples were outgassed for 12 h at 300 °C. The specific surface area (S_{BET}) was calculated by the BET method[25] from the nitrogen adsorption data

in the relative pressure range from 0.06 to 0.11. The total pore volume (V_{TP})[26] was obtained from the adsorbed amount of N_2 at a relative pressure of about 0.99. The external surface area (S_{ext}) and micropore volume (V_{micro}) were estimated using the α_S-plot method (with LiChrospher Si-1000 macroporous silica gel[27] as reference adsorbent) in the p/p^0 range from 0.05 to 0.11. The pore size distribution (PSD) were obtained using the modified Barret–Joyner–Halenda (BJH) method[28] with nitrogen adsorption branch data. Elemental analysis was determined by ICP Varian 715-ES ICP-optical emission spectrometer, after dissolution of the solids in a HNO_3/HF solution. Thermogravimetric analysis (TGA) measurements were done in a Mettler-Toledo TGA/SDTA851E analyzer in air flux with a heating range of 10°C min^{-1}. Field-emission scanning electron microscopy (FESEM) micrographs were recorded on a ZEISS Ultra 55 microscope operating at 2 kV, with a 2 × 10^{-9}. Transmission Electronic Microscopy analysis (TEM) were recorded on a Philips CM10 operating at 100 kV. The samples were ultrasonically dispersed in dichloromethane and dropped to carbon copper grids. Infrared (IR) with absorption of pyridine were performed in a Nicolet 710 FTIR spectrometer using vacuum cells. The measurements were performed in self-supported wafers of 10 mg cm^{-2} that were degassed overnight under vacuum (10^{-4} to 10^{-5} Pa) at 400°C. The spectra were recorded and pyridine was admitted and, after equilibration, the samples were outgassed for 1 h at increasing temperatures (150/250/350 °C). After each desorption step, the spectrum was recorded at room temperature and the background subtracted in the pyridine case and absorption coefficients calculated by Emeis[29] were used. HPLC analysis was performed on a Waters 1525 equipped with RID detector at 35°C and ion exclusion column Coregel 87H3 (7.8 x 300 mm) at 60°C with flow rate of 0.7 mL min^{-1} and H_2SO_4 0.005 mol L^{-1} as mobile phase. Amount of fructose and HMF were determined using external calibration.

Results and discussion

Figure 1 shows the XRD patterns of precursor and calcined MCM-22 samples, as well as the diffractograms of the MWW materials obtained after soft and aggressive swellings treatments and applying different washing cycles. For MWW precursor (P), diffraction 2Θ bands located at 3.3° and 6.6° range corresponding to (001) and (002) reflections, relative to MWW zeolitic layer stacking with thickness of each individual layer of ~2.6 nm, are observed.[30] These layers are connected by hydrogen bonds between silanol groups with the presence of HMI template molecules located between

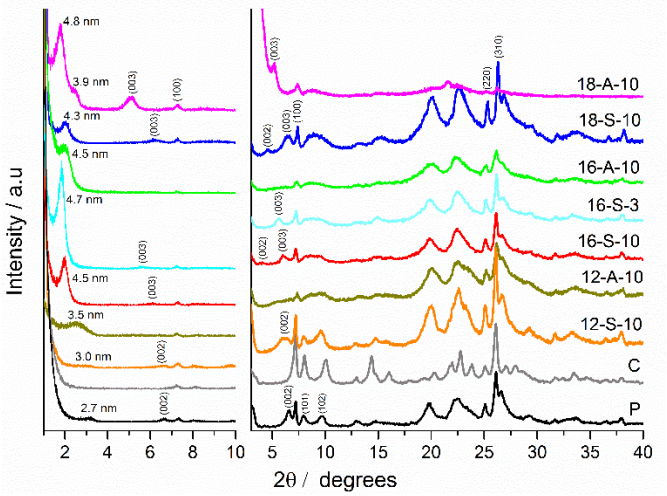

Figure 1. XRD of swelling with $C_{12}TA^+$, $C_{16}TA^+$, $C_{18}TA^+$materials with soft and aggressive procedure.

layers.[31] In addition, intralayer diffraction bands located at 2Θ=7.1° corresponding to (100) diffraction and reflections at higher 2Θ angles, 25.1° and 26.2° assigned to (220) and (310) planes, are also detected. After calcination silanol groups were condensed together with the elimination of interlayer organic template, conventional zeolite *3D*-MCM-22 (C) being obtained.

The Intercalation of swelling agents in layered materials exhibited four mean type-accommodations as lateral monolayer, lateral bilayer, pseudotri-layer and paraffin-type monolayer as showed in Figure 2. This behavior can be monitored by XRD with the increase of basal spacing which is directly related with the thickness of MWW layer, the length of swelling agent and its height of head-group and tail-group. In this case, $C_{18}TA^+$, $C_{16}TA^+$ and $C_{12}TA^+$ have the same height of head and tail-group differentiating them by alkyl-chain length with 2.3, 2.0 and 1.8 nm, respectively, as showed in Figure S2.

The soft swelling treatment using $C_{16}TA^+$ resulted in the overlapping of the (101) and (102) diffraction bands, yielding only a broad peak located between 8° and 10° 2ϴ range. This fact indicated partial loss of vertical alignment order in the stacking direction, *i. e.*, along axis *c*. The molecular dimensions of the swelling agents which are placed in the interlayer space, between individual MWW layers, are shown in Figure 1 and S2. Based on XRD, the sum of length $C_{16}TA^+$ (2.0 nm) and thickness of an individual MWW layer (2.5 nm) should presents a basal spacing estimated with 4.5 nm which leads a surfactant accommodation in paraffin-type monolayer between

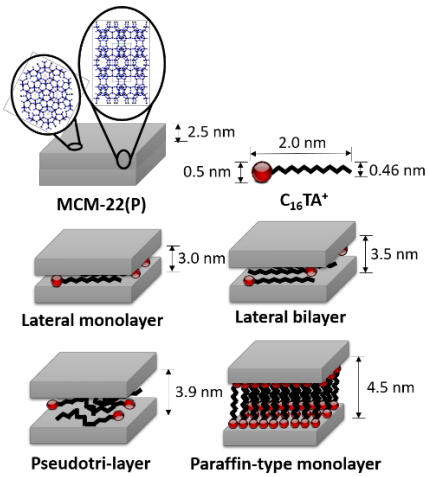

Figure 2. Type-accommodation of $C_{16}TA^+$ (2.0 nm length) swelling agent between MWW layers monitored by XRD. For the basal spacing it was considered the thickness of an individual MWW layer (2.5 nm), the height of head-group surfactant (~0.5 nm) and height of tail-group (~0.46 nm).

MWW layers. The XRD pattern obtained for the sample 16-S-3 showed basal spacing of 4.7 nm estimated from (001) reflection band. The difference of 0.2 nm may related with excess of swelling agent intercalated once than after ten washing cycles the basal spacing was decreased to 4.5 nm, being (002) diffraction band also observed. The presence of TPA^+ and its dimension (0.88 nm, see Figure S2) used with long-alkyl swelling surfactants for swelling may not be excluded of basal spacing value once that is also interacting with the long-alkyl surfactants. However, XRD pattern of swelling MWW with only TPA^+ agent did not show increase of basal spacing consistent with its molecular dimension (see Figure S1).

In terms of MWW structural conservation, XRD patterns show that soft swelling treatment preserved the crystal structure, indicating that room temperature, although working with high basic pH (13.57), minimized fragmentation and dissolution of the silica from zeolitic layers. The intense diffraction bands detected in (100), (220), (310) intralayer peaks and the excellent ordering degree of swelling materials, as it is evidenced by emergence of (002) and (003) basal peaks confirmed that soft swelling conditions better kept MWW structure of the layers, without losing the order along axis *c*.

On the other hand, aggressive swelling 16-A-10 favored a separation between MWW layers with 4.5 nm with a broad (001) diffraction band (compared to 16-S-10) which indicated a marked irregularity in the accommodation of surfactant in paraffin type-monolayer in the interlayer space. Furthermore, aggressive treatment implied lower intensities in the (100), (220) and (310) diffraction bands of swollen materials, showing that partial structural damage of zeolitic structure was occurring. These hypotheses are confirmed both by the absence of repetitive (00l) basal reflections, (002) and (003), indication lower ordering in the separation of the individual layers, and by the presence of broad region in the XRD pattern, between 15-30° 2ɵ, usually assigned to amorphous silica due to the partial dissolution of MWW layers.[17]

The washing cycles carried out after swelling treatments were also evaluated. This step is useful to remove the excess of surfactant which could favor the formation of competitor mesophases, during the consecutive pillarization process. In addition, with this methodology, the pH present in the pillaring synthesis medium could be controlled, avoiding high pHs in the slurry that promotes the rapid polymerization of silica (TEOS) around of the MWW swollen nanocrystals and not only in the interlayer region. Figure 2 shows that increasing washing cycles' number, more effective was the surfactant removing. As consequence, a slight shift of basal (001) (002) and (003) diffraction peaks toward high 2ɵ angles (see XRD patterns of 16-S-3 and 16-S-10 samples) is observed. The high surfactant concentrations (29% wt) used during the swelling step favors the excessive presence of long chain alkyl ammonium molecules in the interlayer space which can be removed during the successive washing cycles due to the weak interaction (H-bonding or Van der Waals) established between them and inorganic layers.

Furthermore, pH values after washing cycles was monitored, as it is indicated in Table S3, being observed that soft swelling procedure kept similar pH values in all cases. In opposite, aggressive swelling treatment resulted in lower pHs associated to formation of deprotonated silicic acids and others oligomeric silicates caused by partial dissolution of zeolitic structure. Similar effect was also founded by Tsapatsis et al.[16] In tenth washing cycle, both pHs achieved close values, although (002) and (003) diffraction bands were not observed in 16-A-10 sample. These results confirmed that aggressive swelling procedure did not favor the regular separation between MWW layers, being necessary an elevated number of furtherly washing cycles to decreased the pH of pillaring media. Thus, soft swelling method preserves better MWW structure of each individual layer without the necessity to carry out too much washing cycles. However, after tenth washing cycle, (002) basal diffraction band was even observed, evidencing the convenience to eliminate the excess of swelling agents through consecutive washing cycles.

For soft swelling treatment, using $C_{12}TA^+$ as intercalation agent, a modest coalescence of (101) and (102) reflection bands was

detected, indicating that non-regular MWW layers separation occurred in vertical alignment, perpendicularly to axis *c*. This fact was confirmed by emergence of broad (002) reflection with (001) diffraction band with basal spacing of 3.0 nm, probably due to the insufficient amount of swelling agent accommodated in form of lateral monolayer between MWW layers. In contrast, aggressive swelling in presence of $C_{12}TA^+$ molecules caused the overlapping of (101) and (102) reflection bands, indicating poor vertical ordering of *c*-stacking crystals. The (001) diffraction band with a broad region is observed with basal spacing of 3.5 nm which suggests a lateral bilayer conformation of swelling agent.

In the case of MWW samples swollen with $C_{18}TA^+$ long chain surfactant (18-S-10 and 18-A-10 samples), some differences were observed comparing its low angle XRD patterns. The 18-S-A-10 sample showed an intense (001) diffraction band with basal spacing of 4.8 nm. Considering the theoretical estimation of molecular dimensions of $C_{18}TA^+$ with 2.3 nm (Figure S2), the basal spacing value is consistent with the molecular dimension of surfactant in paraffin-type monolayer intercalated between individual MWW layers. In addition, (003) diffraction band is observed which indicate a swelling materials with high ordering. Moreover, on the right side of (001) diffraction band, a shoulder is founded with basal spacing of 3.9 nm. This value may indicate that a portion of surfactant in pseudotri-layer accommodation between MWW layers even associated with flexibility and coiling effect that could occurs when a straights-chain hydrophobic groups of surfactant exceeds 16 carbon atoms.[32] Moreover, the high angle XRD pattern indicate a considerable decrease of (100), (220) and (310) diffraction bands which is not only attributed to partial damage of MWW structure treatment with $C_{18}TA^+$ in aggressive swelling but also the increase amount of organic intercalated ($C_{18}TA^+ > C_{16}TA^+ > C_{12}TA^+$) which corroborates with total loss mass observed by TGA of Figure 3 and Table S4 when aggressive swelling . For 18-S-10 sample, the (001) basal spacing with 4.3 nm is lower than expected based on theoretical estimation dimensions of $C_{18}TA^+$. When compared the low angle XRD of both samples (18-S-10 and 18-A-10) the basal spacing value is close to value of the shoulder (with basal spacing of 3.9 nm) present in low angle XRD pattern of 18-A-10 sample, which also suggests a pseudotri-layer accommodation by flexibility and coiling effect of $C_{18}TA^+$ surfactant. Regarding swelling ordering and MWW layer zeolitic preservation, soft swelling with $C_{18}TA^+$ maintain the (002) and (003) reflections which indicates a well ordering degree. In addition, the integrity of MWW layers is preserved by the (100), (220) and (310) diffraction bands that are not drastically affected after swelling.

From TGA and DTG of the derivative MWW samples (Figure 3 and Table S4), different mass losses of swollen materials are observed. In general, increasing washing cycles, the amount of final incorporated surfactant decreased when soft treatments were carried out during the swelling process. Normally, the first loss mass observed at 110 °C, assigned to water adsorbed on surface of materials, was not detected for 16-S-3 sample due to marked

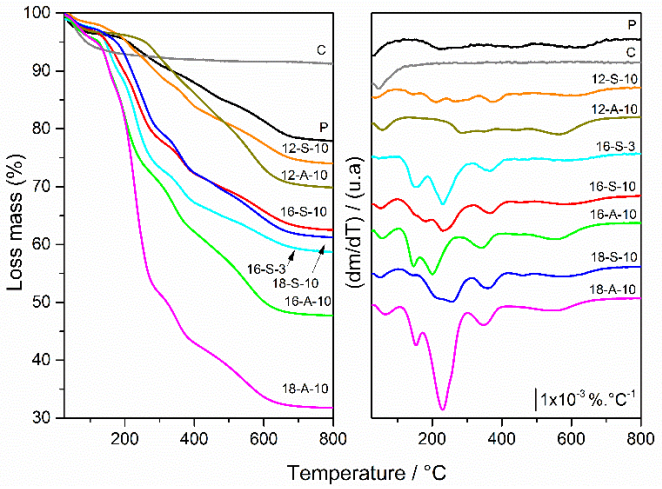

Figure 3. TGA and DTG of swelling with $C_{12}TA^+$, $C_{16}TA^+$ and $C_{18}TA^+$ materials with soft and aggressive procedure.

hydrophobic character of the solid associated to high amount of swelling agent molecules located in the interlayer space.

The main mass loss of this last sample was observed between 180-340 °C, although HMI molecules could also be included into this temperature range come from structural directing agents used during the hydrothermal synthesis of MWW starting precursors. Furthermore, an additional weight loss was detected around 110–180 °C probably associated to some surfactant molecules located outside of interlayer region or weakly interacting with MWW crystals, being more pronounced when the number of washing cycles is higher. In Table S4, weight losses of MWW samples for the different temperature ranges are indicated. In the temperatures range oscillating between 180 °C and 340 °C, long chain ammonium surfactants used as swelling agents and located in the interlayer region, as well as HMI molecules placed in the MWW surface "cups" 12 MR were oxidized, this fact being even favored by the swelling conditions (temperature and pH). Between 340-480 °C, mass loses observed were similar for samples prepared through soft swelling treatments, being assigned to more stabilized HMI molecules

located into the sinusoidal 10 MR microporous channel present in the inner of each individual MWW layer.

In addition, mass loses detected in the temperature range between 480-800 °C were due to residual long chain ammonium surfactants and HMI molecules which were not previously removed, as well as dihydroxylation water produced by condensation phenomenon of surface silanol groups. In the case of swollen 16-A-10 sample, a great amount of organic contribution is detected, even present in the temperature range oscillating between 110-180°C. Probably, the aggressive swelling treatment favored the partial rupture of MWW layers, facilitating that confinement and interaction of swelling agents and HMI molecules with the zeolitic framework was weaker. As consequence, the weight loses from TGA curves were observed at lower temperatures than in the samples swollen through soft conditions, as previously confirmed by XRD and similarly described in literature.[33]

On the opposite, $C_{12}TA^+$ did not exhibit similar mass loses compared with solids swollen with $C_{16}TA^+$ and $C_{18}TA^+$ surfactants. From DTG curves, it is observed that 12-S-10 sample contained only reduced amount of swelling agents intercalated in the interlayer region. In addition, its loss mass is 18% higher than precursor (P) which corroborates with a lateral monolayer conformation of surfactant, as previously confirmed by XRD. For this sample, the mass loss being of 17% in 110-340 °C temperature range. Aggressive swelling treatment for 12-A-10 sample showed a loss mass 27% higher than MWW precursor (P). Furthermore, the total loss mass in 12-A-10 sample is 14% higher than 12-S-10 and may suggests a pseudotri-layer conformation of surfactant as previously showed in XRD results. In the case of 18-S-10 sample, TGA and corresponding DTG are similar to those obtained for 16-S-type materials. Specifically, main weight loss was detected in 180-340 °C temperature range, indicating that large amount of stabilized swelling agents was located in the interlayer region, providing a strong interaction between surface of MWW layers and surfactant molecules which favored well-ordered MWW materials, such as was confirmed from above discussed XRD results. For 18-A-10 sample, this main loss mass associated with the swelling agents was greater than those detected from soft swelling treatments (36%).

In Figure 4, XRD patterns of the MWW derivative materials after pillaring process are shown. For 16-S-10-P material, intense (001) (002) and (003) diffraction peaks are clearly observed, indicating the formation of well-ordered pillared solids with basal spacing of 4.2

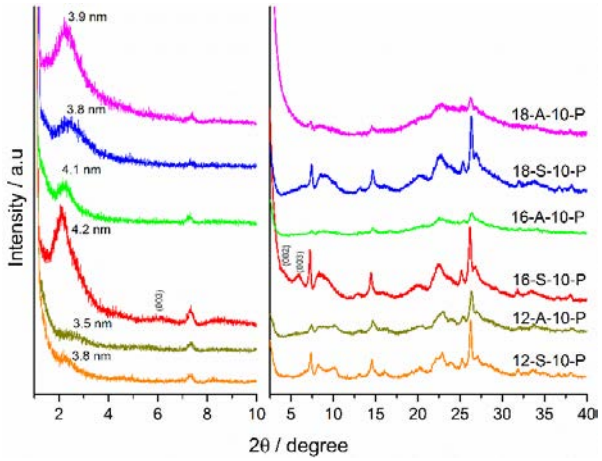

Figure 4. XRD of pillared materials swollen with $C_{12}TA^+$, $C_{16}TA^+$, $C_{18}TA^+$ with soft and aggressive procedure.

nm. XRD diffractogram of pillared 16-A-10-P sample, obtained through aggressive swelling treatment, exhibited (001) basal spacing of 4.1 nm. In addition, the (220) and (310) reflections are slight suppressed after pillaring which is attributed to amorphous silica deposited into material leading to increase the intensity of diffraction region between 15-30° 2ϴ and confirmed by the ICP analysis of Table 1.

XRD patterns of 18-S-10-P shown a broad (001) diffraction peak with basal spacing centered at 3.8 nm which is characterized by absence of basal (002) and (003) peaks that indicates come inhomogeneity on distribution of silica pillars. For 18-A-10-P sample, a broad (001) diffraction band with basal spacing of 3.9 nm was observed. Furthermore, the increase of diffraction region between 15-30° 2ϴ indicate silica incorporation after pillaring which is confirmed by ICP, Table 1.

After pillaring process, XRD patterns of 12-S-10-P and 12-A-10-P samples did not show intense (001) basal peaks, as it early expected by XRD and TGA results of corresponding swollen samples, because negligible amount of $C_{12}TA^+$ surfactant was intercalated between MWW layers associated to lateral monolayer and pseudotri-layer conformation, respectively. However, although with a small presence of surfactant molecules in the interlayer space, MWW materials showed partial disorganization level with small and inhomogeneous pillars, confirmed by broad (001) reflections and moderate coalescence observed between (101) and (102) diffraction peaks.

Nitrogen adsorption isotherms of MWW modified materials are shown in Figure 5. *3D*-MCM-22 (C) zeolite exhibited Type I isotherm with a high adsorbed amount of N_2 at low relative pressures

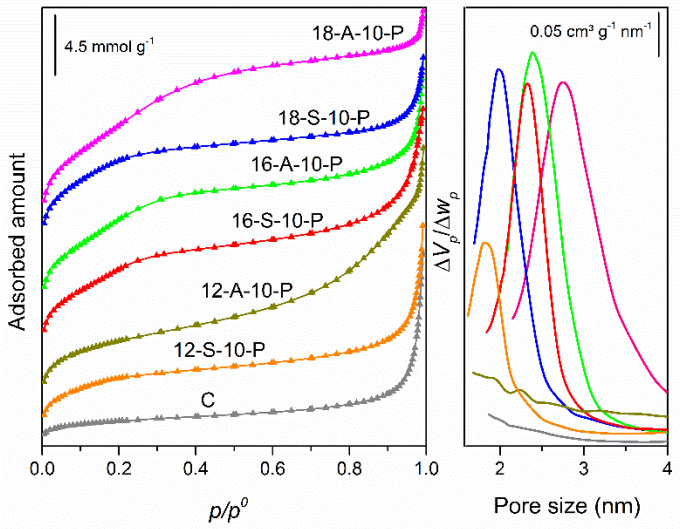

Figure 5. Nitrogen adsorption isotherms and pore size distribution of pillared and modified materials. The isotherms are shifted vertically for the sake of clarity.

(p/p^0 < 0.1) confirmed thus its microporous nature. In prominence, the MWW pillared materials and previously swollen with $C_{18}TA^+$ and $C_{16}TA^+$ swelling agents, showed isotherms with high quantity of N_2 adsorption at low p/p^0 (due to strong adsorbate-adsorbent interactions and/or filling micropores), and a step adsorption between 0.12 and 0.4 of p/p^0 corresponding to the capillary condensation phenomena occurred in the mesoporous region created by pillaring. In the case of isotherms of the 12-A-10-P and 12-S-10-P samples, the N_2 adsorption at low pressures is due to mainly to the presence of micropores in these materials. In addition, the isotherm of the 12-A-10-P sample exhibit a progressive increase of the quantity of N_2 adsorption at relative pressures higher than 0.35, which is associated to mesoporosity present in MWW structure caused by desilication phenomenon. Pore size distribution (Figure 5, right side), of the samples under study showed pore sizes (PS) ranging between supermicropores and small mesopores. In the case of 12-S-10-P sample PS between 1.5-2.2 nm were found, on the contrary, the 12-A-10-P sample did not show pores in the pillar sizes range. For the 18-S-10-P and 18-A-10-P samples PSD ranges between 1.6-2.5 nm and 2.1-4.0 nm were found, respectively. Instead, for 16-S-10-P and 16-A-10 pillared samples the PS ranges between 1.8-2.5 nm and 1.8-2.8 nm were found. In a general form, it was observed aggressive swelling treatment and subsequent pillaring generate materials with broader pore size distributions.

Textural properties results are shown in Table 1 for the MWW-type samples obtained after pillaring procedure, being observed a significant increase in the specific surface area and pore volume of all pillared samples compared with standard *3D*-MWW zeolite (C). Firstly, solids swollen with longer hydrocarbon length chain agents exhibited higher surface area and accessibility. The pillared MWW materials prepared after swelling process using $C_{12}TA^+$ surfactants showed a certain increase in the specific surface area and partial disruption along *c*-stacking direction compared with 3D-MWW (C) zeolite and a modest pillaring for 12-S-10-P sample. For pillared MWW materials previously swollen with $C_{16}TA^+$ molecules through soft or aggressive swelling treatments marked an increase in the specific surface area of approximately 54% compared with *3D*-MCM-22 (C) zeolite. Similarly, for 18-S-10-P and 18-A-10-P pillared materials, an increase in the specific surface area of ~62% front of MCM-22 (C) was observed. This fact clearly evidenced that pillaring process was successful after soft and aggressive swelling treatments. Respect to micropores, the sample obtained with aggressive swelling and pillaring with $C_{18}TA^+$ showed the absence of micropores and followed by $C_{16}TA^+$ which presents small quantity of micropores (0.01 cm^3g^{-1}). This indicates aggressive treatment may obstruct the microporous structure of individual MWW layers due to silicon (deposit on MWW layers) from pillaring process may block the micropores. This effect is supported when 18-A-10-P is compared to aggressive swelling and pillaring sample 12-A-10-P which is desilicated (no silica was incorporated from pillaring) which maintains significant microporosity and increased the interparticle pore volume (V_{int}) compared with *3D*-MWW zeolite (C). The possibility of formation of competing mesophases (type M41S, MCM-41) in swelling medium of 18-A-10 was also take into account. It well know that basic medium with surfactant, silicon and aluminum sources (which would be supplied from MWW layers) are the mean reactants to M41S formation. However, if a mesophase was formed, the presence of diffraction bands in low angle XRD pattern should be maintained after direct calcination of swollen 18-A-10 sample. The swollen 18-A-10 sample was calcined and no XRD diffraction bands characteristics of mesophases were found (see Figure S5). Moreover, diffraction bands characteristic of MWW zeolite are present in 18-A-10-P and the catalytic activity showed that microporosity still existing.

In Table 1, Si/Al molar ratios of materials after swelling (in parenthesis) and pillarization post-synthesis treatments is shown. The starting zeolitic precursor MCM-22(P) presented Si/Al molar ration of 22, decreasing after swelling process which indicated that partial dissolution of some silica units from individual MWW layers.

Table 1. Textural properties of pillared and modified materials with different surfactant sizes and swelling procedures.

Material	Si/Al (ICP)	XRD 2θ (°)	XRD d_{001} (nm)	S_{BET} (m^2g^{-1})	S_{ext} (m^2g^{-1})	V_{TP} (cm^3g^{-1})	V_{micro} (cm^3g^{-1})	V_{int}** (cm^3g^{-1})
C	(22) 21	(3.3)	(2.7)	520	140	0.63	0.15	0.39
12-S-10-P	(18) 28	(3.9) 2.3	(3.0) 3.8	685	440	0.67	0.10	0.34
12-A-10-P	(8) 9	(2.7) 2.4	(3.2) 3.5	710	460	0.77	0.11	0.43
16-S-10-P	(18) 34	(1.9) 2.1	(4.5) 4.2	795	670	0.76	0.05	0.33
16-A-10-P	(10) 39	(1.9) 2.1	(4.5) 4.1	800	760	0.73	0.01	0.29
18-S-10-P	(18) 26	(2.0) 2.2	(4.3) 3.8	840	750	0.61	0.04	0.20
18-A-10-P	34	(1.8; 2.3) 2.3	(4.8; 3.9) 3.9	850	850	0.65	--	0.13

* Values in parenthesis correspond to the swollen materials.
** The interparticle pore volume (V_{int}) was obtained from the difference between V_{TP} (obtained at 0.99 of p/p^0) and the pore volume obtained at 0.6 of p/p^0. This value correspond to pore volume of sizes from 4 to 100 nm.

This decrease was more marked for aggressive than for soft swelling treatments. After pillaring process, Si/Al molar ration increased due to intercalation in the interlayer space of silica pillars, being more pronounced when $C_{16}TA^+$ and $C_{18}TA^+$ surfactants were used as swelling agents (see XRD in Figure 4). For 18-A-10-P sample, Si/Al molar ratio of 34 presents similar value with the pillared samples 16-S-10-P and 16-A-10-P and 18-A-10-P indicate the participation of silica into product. MWW swollen material obtained through soft swelling treatment using $C_{12}TA^+$ surfactant exhibited Si/Al molar ration of 18, being similar to others MWW swollen solids also prepared through soft swelling treatments. After pillaring this sample, 12-S-10, the lowest swelling agent amount finally incorporated (see TGA results) was involved with TEOS in the interlayer region, leading to increase Si/Al molar ration up to 28.

In contrast, aggressive swelling treatment (12-A-10) drastically dissolved part of the silica from MWW layers, achieving Si/Al=8 which was maintained after pillaring process (Si/Al=9). Indeed, a decrease of 55% yield was founded after aggressive swelling procedure. However, in the pillared sample (12-A-10-P), microporous volume was not effectiveness altered, being close to calcined *3D*-MCM-22 zeolite. This fact would be explained by lower amount of quaternary ammonium surfactant present in the interlayer space together with shorter terminal hydrocarbon chain, which prevented the effective intercalation of TEOS units to form ordering silica pillars. The fact by swelling with $C_{12}TA^+$ not be as effective with other swelling agents as $C_{18}TA^+$ and $C_{16}TA^+$ may lie in its lower capacity to form rod-like micelles, which is less favored for shorter surfactant lengths. Moreover, the instability to form of $C_{12}TA^+$ rod-like micelles increase above 70 °C.[34] This may be associated to desilication phenomenon occurred in 12-A-10-P sample.

In Figure 6, morphology of 2D zeolitic precursor of MCM-22 (P) (image *a*) and 3D calcined MCM-22 (C) (image *b*) are shown from SEM microscopy. In both cases, hexagonal disk-shaped crystals of average sizes of ~1.4 μm were observed by successive vertical stacking growth of MWW layers. Comparing images 6a and 6b, flat plates were observed after calcination process due to surface silanol condensation phenomenon.

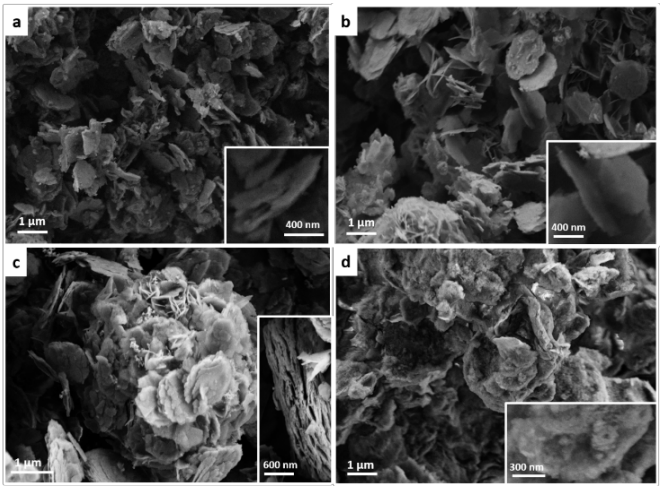

Figure 6. SEM analysis of precursor P(a) and MCM-22 zeolite C (b). Images (c) and (d) corresponding to 12-S-10-P and 12-A-10-P materials, respectively.

SEM micrographs of pillared MWW material, previously swollen with $C_{16}TA^+$ and $C_{18}TA^+$ surfactant molecules, are shown in Figure 7. In the case of samples obtained from soft swelling process, MWW layers integrity was maintained (images *a* and *c*). In addition, analyzing the *c*-stacking of disk-shaped crystals (see insets in Figure 7), both samples showed more expanded particles than *3D*-MCM-22 (Figure 6b). Disruption of some MWW crystals together with

particles sizes decrease, a partial amorphization being also observable.

Pillared 18-A-10-P sample obtained after aggressive swelling process using $C_{18}TA^+$ surfactant, exhibited aggregation phenomena of curved disk-shaped crystals with presence of non-zeolitic component in form of amorphous silica which is attributed to dissolution of MWW layers after aggressive swelling and residual silica which may not participate of the pillars between MWW layers. Micrographs showed in Figure S5 confirms this hypothesis .

TEM images in Figure 8a and b show the *c*-stacking phenomenon of zeolitic layers both in the MWW precursor (P) and in the corresponding calcined MCM-22 (C) zeolite. The measures of Figure 7a correspond to sizes of one (2.82 nm), two (5.64 nm), or five (14.1 nm) consecutive MWW layers (see insets in Figure 8a). After calcination process of MWW precursor, elimination of interlamelar and intracrystalline structural directing agent molecules together with external silanol condensation between contiguous MWW layers was also observed, being measured the stacking of four (10 nm) connected MWW layers (Figure 8b). Furthermore, microporous 10 MR channels (~0.6 nm) present between the individual layers, detected by white regions in the TEM micrographs, were clearly observed.

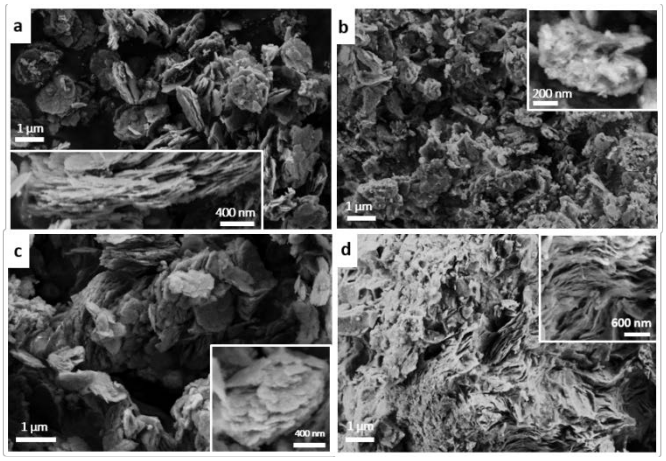

Figure 7. SEM analysis of 16-S-10-P (a) and 16-A-10-P (b). Images (c) and (d) corresponding to 18-S-10-P and 18-A-10-P materials respectively.

Figure 8c shows TEM imagens of pillared 16-S-10-P sample, being detected eight MWW layers separated by silica pillars. The measure with approximately 4.4 nm comprises the sum of the thickness of one MWW layer (2.5 nm) added to interlayer spacing created by pillars (~1.9 nm). The measure with ~1.8 nm comprises the interlayer spacing between two MWW layers which are consistent with basal spacing of XRD patterns of pillared 16-S-10-P. TEM micrographs of pillared 16-A-10-P is shown in Figure S6, being difficult to observe separated MWW layers by silica pillars due to aggressive swelling process carried out which produced partial damage of zeolitic crystals added the fact of amorphous silica is present by pillaring process. For the sample 12-A-10-P desilication phenomena were observed by TEM of Figure S7 where mesoporous regions are opened in particle crystals.

The 18-A-10-P sample obtained through aggressive swelling and pillaring treatments in presence of $C_{18}TA^+$ surfactant and TEOS, showed aggregation phenomena (see inset Figure 8d) being difficult to find separated layers by silica pillars. However, it is observed single curved, separated and disordered zeolitic MWW layers. TEM analysis of Figure S8 compares the morphology of 3D-MCM-22 (C) which has flat, clean and smooth crystals with the coarse aspect of both 18-S-10-P and 18-A-10-P samples to confirm the change of morphology and the presence of amorphous silica into pillared products being this effect more visible in 18-A-10-P sample.

Figure 9 shows a general scheme summarizing the dimensions influence of swelling agents used during soft or aggressive conditions on the final MWW pillared materials. It was observed that behavior surfactants between MWW layers directly depends of the length of surfactant alkyl-chain and the type of swelling treatment (soft or aggressive) which conducts to four different surfactant type-accommodations. Soft swelling with $C_{12}TA^+$ conducts to lateral type monolayer accommodation of surfactant confirmed by XRD and TGA analysis. After pillaring it was observed a gently and almost negligible increase of basal spacing together with a moderate coalescence of (101) and (102) diffraction bands by partial loss of vertical alignment order in the stacking direction along axis *c*. This features added with moderate increase of silica after pillaring, the be of specific surface maintaining its microporous surface and pore size ranging close to small mesopores region conducts a disordered/pillaring material. Aggressive swelling $C_{12}TA^+$ exhibited lateral bilayer conformation together with desilication phenomenon attributed to temperature of swelling and $C_{12}TA^+$ micelle instability at 80 °C. The decrease of Si/Al ratio = 9 of swollen maintaining similar value after pillaring indicates large mesopores created not by robust pillars between MWW layers but for removal some MWW units from particle crystals as observed by TEM and isotherm analysis.

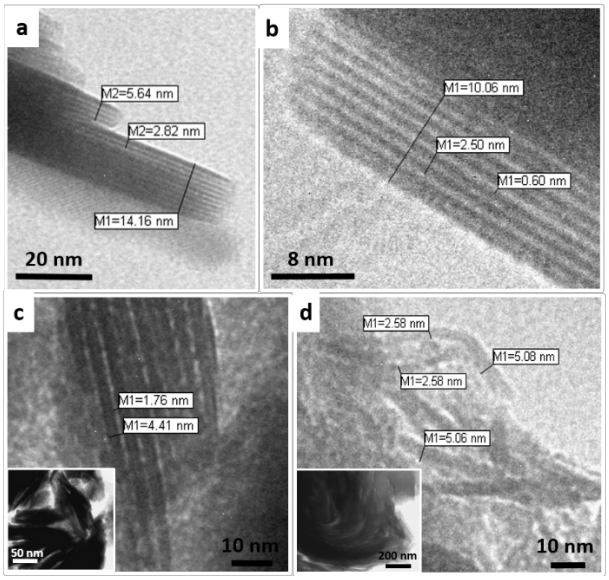

Figure 8. TEM of MWW precursor (P) (a), MCM-22 (b) and pillaring samples 16-S-10-P (c) and 18-A-10-P (d).

Swelling with $C_{16}TA^+$ surfactant lead to paraffin-type monolayer accommodation both soft and aggressive swelling formed pillared materials with basal spacing of centered at 4.2 and 4.1 nm, respectively. Soft swelling and pillaring material possesses more ordering as observed by presence of (002) and (003) diffraction bands.

Swelling with $C_{18}TA^+$ lead to paraffin-type monolayer accommodation with aggressive swelling with a portion of swollen with pseudotri-layer conformation between layers which may attributed to coiling and flexibility effect of $C_{18}TA^+$. The pillared form showed a decrease of basal spacing (5.0 nm to swollen going to 3.9 nm after pillaring) with a broad (001) diffraction band may associated to inhomogeneous pillar distributions which conducts of more mesoporous formation in a broad range. Moreover, the microporosity of MWW layers was drastically affected by aggressive swelling where no values of microporous surface and volume are presented together with a considerable quantity of amorphous silica into material as observed by TEM analysis. Soft swelling with $C_{18}TA^+$ presents pseudotri-layer surfactant accommodation between MWW layers which is attributed to coiling and flexibility behavior of $C_{18}TA^+$. Its pillared form showed a basal spacing centered at 3.8 nm.

Alternatively, surface properties of pillared MWW materials were investigated by FTIR spectroscopy through adsorption-desorption of pyridine. Figure 10 shows the FTIR spectra in the hydroxyl region of MWW pillared materials, being detectable vibration bands at ~3620 cm^{-1} and 3670 cm^{-1} which correspond to surface bridged hydroxyl groups associated to framework Al–OH–Si and extra-framework aluminum species generated upon calcination process, respectively. Furthermore, the vibration bands centered at ~3730 and ~3748 cm^{-1} were assigned to internal and external silanol groups, respectively.[35]

In detail, vibration band at ~3620 cm^{-1} (BAS) is clearly detectable in the spectra of calcined 3D-MCM-22 and pillared 16-S-10-P samples, confirming that bridged hydroxyl groups (Al-OH-Si) are preserved after soft swelling and consecutive pillaring processes.[36] At the meantime, vibration band intensity located at 3748 cm^{-1}, assigned to the presence of external silanol groups, was notably increased for 16-S-10-P and 16-A-10-P samples due to intercalated silica pillars placed in the interlayer space. Moreover, vibration bands centered at ~3729 cm^{-1}, associated to surface silanol groups, decreased after pillaring process, indicating that silica pillars interacted with external silanol groups present in the MWW layers.

All pillared MWW materials contained acid sites with different strength which were detected using pyridine as adsorbed probed molecules (values in Table S10). Specifically, vibration bands at 1610 cm^{-1} (also 1453 cm^{-1}) and 1544 cm^{-1} (also and 1635 cm^{-1}) are characteristics of pyridine adsorbed on Lewis (LAS) and Brönsted (BAS) acid sites, respectively. In addition, vibration band observed at 1447 cm^{-1} is assigned to hydrogen bonded species by interaction with hydroxyl groups on the zeolite surface.[36]

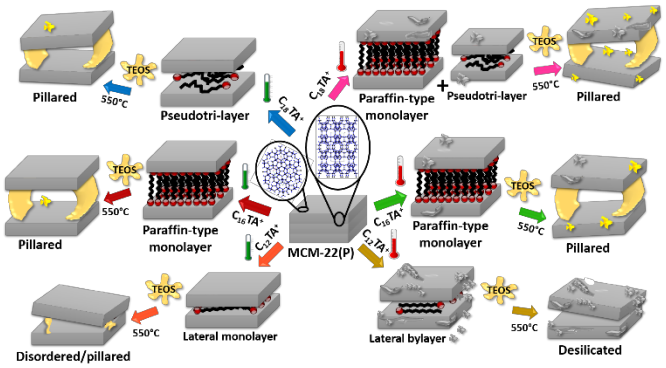

Figure 9. General scheme of surfactant accommodation between layers of swelling and pillaring MWW materials. Red or green thermometers (aggressive or soft swelling). The colored arrows represents the surfactant sizes. Pink/blue ($C_{18}TA^+$), red/green ($C_{16}TA^+$) and orange/mustard ($C_{12}TA^+$).

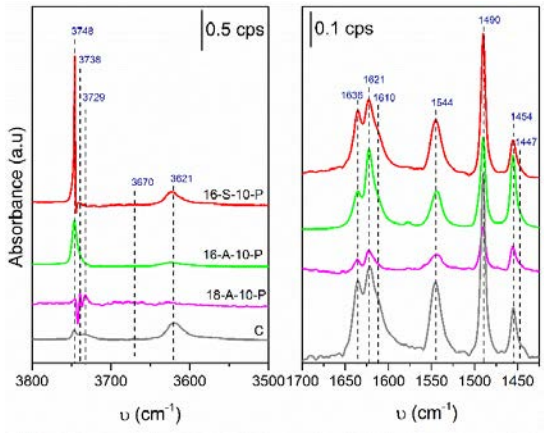

Figure 10. FTIR after outgassing at 400 °C for 2 hours and spectra after pyridine adsorption at 150°C. Spectra are normalized to 11.3 mg sample.

The IR spectra showed that the intensity band focused on 1544 cm^{-1} decreased after pillaring process which indicated that the number of BAS was "diluted" by insertion of silica pillars. This decreasing is pronounced in materials obtained through aggressive swelling treatment 16-A-10-P and more significantly to 18-A-10-P sample that possesses more disordered pillar and favored partial amorphization of the MWW layers which suggests considerable non-zeolitic component. On the other hand, LAS estimated by the vibration band intensity centered at 1454 cm^{-1} was higher for 16-A-10-P sample due to aluminum extra-framework present in the solid after aggressive swelling and consecutive pillarization post-synthesis treatments.

The characterization results showed that through the combined action of swelling conditions (soft or aggressive) and interlamelar agents, with different molecular dimensions, modulation of physico-chemical and morphological nature of derivative MWW-type materials is possible. Different accessibility level achieved together with preserved acidity in the obtained MWW pillared zeolites open the possibility to analyze and evaluate these materials from catalytic point of view.

Catalytic activity

Recently, great efforts has been made on effective routes for the synthesis of 5-HMF from C6-based carbohydrates. This demand comes from the necessity to obtain new sustainable fuels sources and chemicals through inexpensive and renewable materials with high added-value, proposing alternative efficient industry processes which could replace the limited fossil fuels.[37,38] Specifically, 5-HMF is a valuable biomass-derived platform intermediate, which is potentially used as fuel and additives in fine chemicals, pharmaceuticals and polymers.[39,40,41,42]

The use of solid acid catalyst for dehydration carbohydrates has several advantages over liquid acid catalyst, such as easier separation, being recoverable and recyclable for successive reuses. Moreover, adjusting surface acidity of heterogeneous solid catalyst, selectivity to desired product can be achieved at shorter times, working with higher temperatures, voiding corrosion and safety problems.[43,44] Acid H-Y, H-ZSM-5, H-mordenite, H-β, β-dealuminated has been used to produce 5-HMF from carbohydrates.[45,46,47,48] In addition, layered zeolites are one the most potential and promising materials to replace current used catalysts and advancement areas of study on porous and hierarchical materials.[49] Take into account, acid pillared MWW materials, previously described, with different porosity levels and morphology in function of surfactant agents dimensions and swelling conditions (soft or aggressive) were evaluated as active catalysts for dehydration carbohydrates to 5-HMF production. In addition, has been demonstrated that the combined action between Brønsted and Lewis acid sites were highly beneficial to 5-HMF production.[50] Thus, fructose dehydration would be *a priori* an ideal model substrate to evaluate the performance of pillared MWW catalytic materials for biomass conversion.[51]

In fact, molecular size of fructose (0.85 nm) and 5-HMF (0.59 nm) limits their access and diffusion through internal two-dimensional 10 MR sinusoidal channels of MWW zeolite (0.40 x 0.55 nm), the reaction being presumably carried out in external active sites located in the surface of MWW individual layers. Figure 10 shows fructose conversion and 5-HMF yield using MWW materials as heterogeneous catalysts. Blank test reaction (without solid catalyst) led 8% and 15% of yield for 5-HMF after 1 and 3 h, respectively, similarly to those reported in the bibliography for the same reaction conditions.[52] In our case, all MWW materials were active to fructose dehydration, reaching conversions close to 100% after 3 h.

Table 2. Rates of 5-HMF production over various MWW-type derivative materials.

Catalyst	Rate of HMF production, (μmol min^{-1})[a]	Catalyst loading, (μmol H^+)[b]	TOF, (min^{-1})
C	23	72.7	0.31
12-S-10-P	23.8	-	-
16-S-10-P	37.7	56	0.67
16-A-10-P	19.9	59.2	0.33
18-A-10-P	37.2	21.2	0.56

[a] rates of HMF production were taken from Supplementary Information, Figure S11. [b] acidity values at 150 °C (BAS + LAS) were taken from Supplementary Information, Table S10.

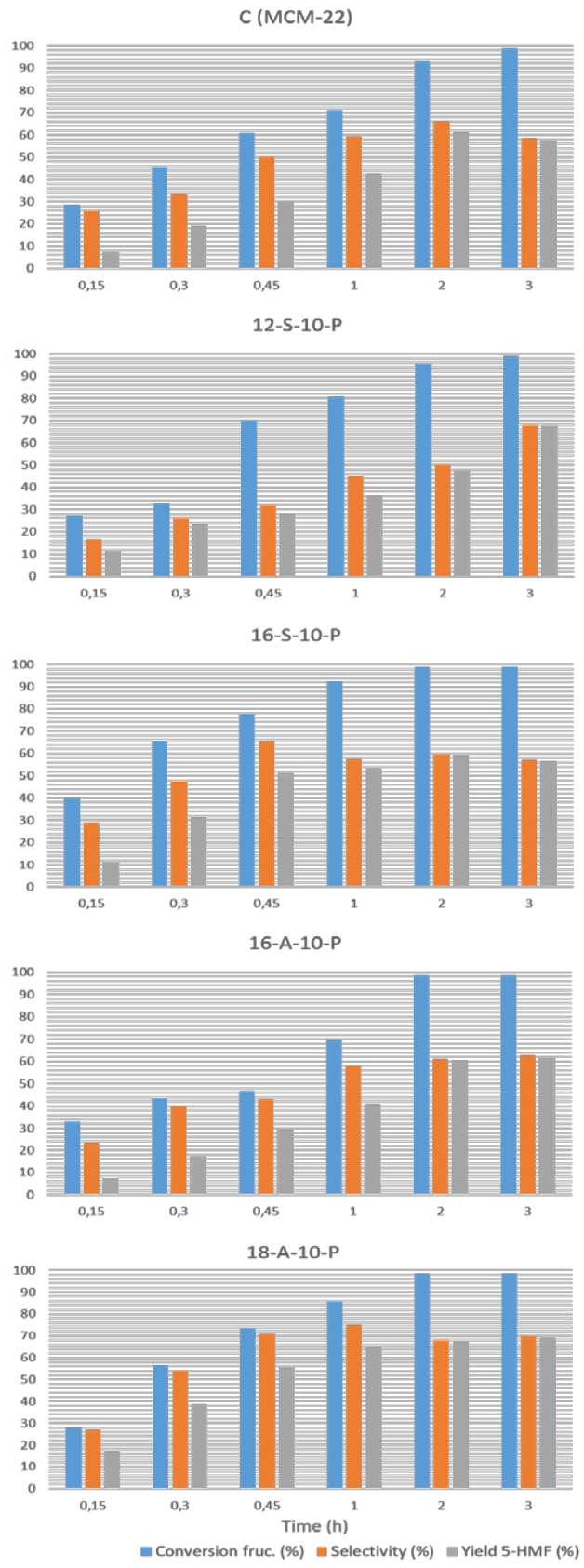

Figure 11. Fructose conversion, selectivity and 5-HMF-5 yield over C (MCM-22), 12-S-10-P, 16-S-10-P, 16-A-10-P and 18-A-10-P MWW-derivative materials.

Conventional 3D MCM-22 zeolite (C) showed 61% of yield for 5-HMF in 2 h, confirming that probably certain diffusional problems limit the reaction process, being performed in the external surface of zeolite crystals. However, the obtained yield was higher compared with other microporous commercial β zeolite and similar to hollow microspherical β zeolites (63%).[46,53] After 3 hours of reaction, 5-HMF yield progressively decreased up to 57% after 5 h (not shown). This tendency was due to cocking formation on active sites or secondary reactions which rehydrate final product, forming presumably insoluble humins (brown products were visible at final of reaction), formic acid and levulinic acid. Indeed, levulinic acid was identified between 2-5 h of reaction process.

Specifically, disordered/pillared 12-S-10-P material showed a yield of 68% for 5-HMF within 3 h of reaction. The high activity achieved can be due to order absence of MWW layers perpendicularly aligned to axis *c* which partially opened external surface of 12 MR supercages, previously inaccessible in the 3D calcined MCM-22 (C). This effect increased external surface and accessibility of the pillared material, being preserved the starting MWW structure and the Si/Al molar ration (Si/Al= 28). However, levulinic acid was identified, as well as a decrease of 7% in the 5-HMF yield after 1 h and 3 h of reaction, respectively.

In the case of pillared 16-S-10-P, 16-A-10-P and 18-A-10-P materials, maximum conversion and yield were reached within 2 h of reaction because swelling, pillaring improved catalyst accessibility and reactant diffusion of reactant and products to active sites. In detail, higher conversion and yield was achieved for pillared 16-S-10-P sample and 18-A-10-P samples within 45 min of reaction. Indeed, turnover frequencies (TOF, Table 2) showed highest activities for both materials. Even, 16-S-10-P material which exhibited lower specific surface area, achieved higher performance (78% for fructose conversion and 51% for 5-HMF yield) than 16-A-10-P sample (46% and 30%, respectively). This difference may due to higher MWW layer integrity obtained in the pillared materials swollen through soft conditions that avoided structure amorphization. Hence, soft swelling treatment favored the formation of more robust (without amorphous phases), accessible and active pillared MWW catalysts.

The highly disordered pillared 18-A-10-P sample showed best performance within 1 h of reaction, reaching 85% and 65% for fructose conversion and 5-HMF yield, respectively. Even, although acidity decreased (Table S10), 18-A-10-P material showed higher

catalytic activity associated to larger pore size distribution (2.1 – 4.0 nm) formed by pillaring (layers which increased the access to active sites located in the external supercages. As result, dehydration was favored, facilitating products diffusion and achieving higher 5-HMF yield (67%) than 16-S-10-P within 2 h of reaction and maximal yield within 3h (69%). The DTG (see Figure S12) for pillared MWW materials used as catalysts and recovered after 5 h of reaction showed total weight loses of 25, 20, 20, 23 and 28% for 3D calcined MCM-22, 12-S10-P, 16-S-10-P, 16-A-10P and 18-A-10 samples, respectively. These values confirmed that partial deactivation of the catalysts could occur, being associated to cocking formation and consequent coke deposition on active sites, this effect being more acute for highly disordered pillared 18-A-10-P sample where active sites were more accessible.

Conclusions

We have demonstrated that surfactant molecular dimensions play a key role during the swelling of MWW precursors, generating a valid alternative route to obtain derivative MWW-type zeolites with controlled physico-chemical and morphological nature, being possible to establish both accessibility level and associated acidity through desilication effect. Soft and aggressive treatments, using $C_{12}TA^+$ as swelling agent, produce partial disordered/pillared materials, and in the case of aggressive methodology, even desilication. Swelling with $C_{16}TA^+$ surfactant leads pillared materials with minimal structure damage by soft swelling. Aggressive swelling with $C_{16}TA^+$ and $C_{18}TA^+$ create pillared MWW with more mesoporosity range and structure damage. The MWW materials demonstrate potential use for fructose conversion, especially highly disordered pillared MWW-type zeolites which exhibited higher 5-HMF yield in just 45 min of reaction.

Acknowledgements

We are grateful to CAPES Foundation and PDSE program (process number 99999.004779/2014-02) from Ministry of Education of Brazil. U.D and A.C acknowledge to the Spanish Government (Severo Ochoa program SEV-2012-0267 and MAT2014-52085-C2-1-P) and to the Generalitat Valenciana (Prometeo) by the funding. The European Union is also acknowledged by ERC-AdG-2014-671093 – SynCatMatch.

References

1. T. Maesen, in *Studies in Surface Science and Catalysis*, eds. H. v. B. A. C. Jiří Čejka and S. Ferdi, Elsevier, 2007, vol. Volume 168, pp. 1-12.
2. A. Corma, *Chemical Reviews*, 1997, **97**, 2373-2420.
3. C. S. Cundy and P. A. Cox, *Chemical Reviews*, 2003, **103**, 663-702.
4. M. E. Davis, *Nature*, 2002, **417**, 813-821.
5. K. Li, J. Valla and J. Garcia-Martinez, *ChemCatChem*, 2014, **6**, 46-66.
6. J. Perez-Ramirez, C. H. Christensen, K. Egeblad, C. H. Christensen and J. C. Groen, *Chemical Society Reviews*, 2008, **37**, 2530-2542.
7. K. Na, M. Choi and R. Ryoo, *Microporous and Mesoporous Materials*, 2013, **166**, 3-19.
8. Y. Yan, X. Guo, Y. Zhang and Y. Tang, *Catalysis Science & Technology*, 2015, **5**, 772-785.
9. A. Corma, U. Díaz, T. García, G. Sastre and A. Velty, *Journal of the American Chemical Society*, 2010, **132**, 15011-15021.
10. U. Díaz, Á. Cantín and A. Corma, *Chemistry of Materials*, 2007, **19**, 3686-3693.
11. W. J. Roth, C. T. Kresge, J. C. Vartuli, M. E. Leonowicz, A. S. Fung and S. B. McCullen, in *Studies in Surface Science and Catalysis*, eds. H. G. K. I. K. H.K. Beyer and J. B. Nagy, Elsevier, 1995, vol. Volume 94, pp. 301-308.
12. A. Corma, V. Fornés, A. Chica and U. Diaz, *EP Spanish Patent 9802283,* 1999.
13. K. Na, M. Choi, W. Park, Y. Sakamoto, O. Terasaki and R. Ryoo, *Journal of the American Chemical Society*, 2010, **132**, 4169-4177.
14. X. Zhang, D. Liu, D. Xu, S. Asahina, K. A. Cychosz, K. V. Agrawal, Y. Al Wahedi, A. Bhan, S. Al Hashimi, O. Terasaki, M. Thommes and M. Tsapatsis, *Science*, 2012, **336**, 1684-1687.
15. W. J. Roth and J. Cejka, *Catalysis Science & Technology*, 2011, **1**, 43-53.
16. S. Maheshwari, E. Jordan, S. Kumar, F. S. Bates, R. L. Penn, D. F. Shantz and M. Tsapatsis, *Journal of the American Chemical Society*, 2008, **130**, 1507-1516.
17. S. Maheshwari, C. Martínez, M. Teresa Portilla, F. J. Llopis, A. Corma and M. Tsapatsis, *Journal of Catalysis*, 2010, **272**, 298-308.
18. W. J. Roth and J. C. Vartuli, in *Studies in Surface Science and Catalysis*, eds. A. Sayari and M. Jaroniec, Elsevier, 2002, vol. Volume 141, pp. 273-279.

19. W. J. Roth, J. Čejka, R. Millini, E. Montanari, B. Gil and M. Kubu, *Chemistry of Materials*, 2015, **27**, 4620-4629.
20. M. Mazur, P. Chlubná-Eliášová, W. J. Roth and J. Čejka, *Catalysis Today*, 2014, **227**, 37-44.
21. M. Shamzhy, M. Mazur, M. Opanasenko, W. J. Roth and J. Cejka, *Dalton Transactions*, 2014, **43**, 10548-10557.
22. V. J. Margarit, M. E. Martínez-Armero, M. T. Navarro, C. Martínez and A. Corma, *Angewandte Chemie International Edition*, 2015, **54**, 13724-13728.
23. H. Y. Luo, V. K. Michaelis, S. Hodges, R. G. Griffin and Y. Roman-Leshkov, *Chemical Science*, 2015, **6**, 6320-6324.
24. A. Corma, C. Corell and J. Pérez-Pariente, *Zeolites*, 1995, **15**, 2-8.
25. S. Brunauer, P. H. Emmett and E. Teller, *Journal of the American Chemical Society*, 1938, **60**, 309-319.
26. K. S. W. Sing, D. H. Everett, R. A. W. Haul, L. Moscou, R. A. Pierotti, J. Rouquerol, T. Siemieniewska and *Pure Appl. Chem*, 1985, **57**, 603–619.
27. M. Jaroniec, M. Kruk and J. P. Olivier, *Langmuir*, 1999, **15**, 5410-5413.
28. J. Villarroel-Rocha, D. Barrera and K. Sapag, *Microporous and Mesoporous Materials*, 2014, **200**, 68-78.
29. C. A. Emeis, *Journal of Catalysis*, 1993, **141**, 347-354.
30. M. A. Camblor, A. Corma, M.-J. Díaz-Cabañas and C. Baerlocher, *The Journal of Physical Chemistry B*, 1998, **102**, 44-51.
31. M. Polozij, H. V. Thang, M. Rubes, P. Eliasova, J. Cejka and P. Nachtigall, *Dalton Transactions*, 2014, **43**, 10443-10450.
32. M. J. Rosen, in *Surfactants and Interfacial Phenomena*, John Wiley & Sons, Inc., 2004, DOI: 10.1002/0471670561.ch3, pp. 105-177.
33. Y. J. He, G. S. Nivarthy, F. Eder, K. Seshan and J. A. Lercher, *Microporous and Mesoporous Materials*, 1998, **25**, 207-224.
34. Q. Huo, D. I. Margolese, U. Ciesla, D. G. Demuth, P. Feng, T. E. Gier, P. Sieger, A. Firouzi and B. F. Chmelka, *Chemistry of Materials*, 1994, **6**, 1176-1191.
35. P. Matias, J. M. Lopes, S. Laforge, P. Magnoux, P. A. Russo, M. M. L. Ribeiro Carrott, M. Guisnet and F. Ramôa Ribeiro, *Journal of Catalysis*, 2008, **259**, 190-202.
36. S. Laforge, P. Ayrault, D. Martin and M. Guisnet, *Applied Catalysis A: General*, 2005, **279**, 79-88.
37. A. Corma, S. Iborra and A. Velty, *Chemical Reviews*, 2007, **107**, 2411-2502.
38. S. P. Teong, G. Yi and Y. Zhang, *Green Chemistry*, 2014, **16**, 2015-2026.
39. Y. Roman-Leshkov, C. J. Barrett, Z. Y. Liu and J. A. Dumesic, *Nature*, 2007, **447**, 982-985.
40. A. A. Rosatella, S. P. Simeonov, R. F. M. Frade and C. A. M. Afonso, *Green Chemistry*, 2011, **13**, 754-793.
41. M. J. Climent, A. Corma and S. Iborra, *Green Chemistry*, 2011, **13**, 520-540.
42. A. Gandini and M. N. Belgacem, *Progress in Polymer Science*, 1997, **22**, 1203-1379.
43. X. Tong, Y. Ma and Y. Li, *Applied Catalysis A: General*, 2010, **385**, 1-13.
44. J. J. Bozell and G. R. Petersen, *Green Chemistry*, 2010, **12**, 539-554.
45. C. Moreau, R. Durand, S. Razigade, J. Duhamet, P. Faugeras, P. Rivalier, P. Ros and G. Avignon, *Applied Catalysis A: General*, 1996, **145**, 211-224.
46. K.-i. Shimizu, R. Uozumi and A. Satsuma, *Catalysis Communications*, 2009, **10**, 1849-1853.
47. R. O'Neill, M. N. Ahmad, L. Vanoye and F. Aiouache, *Industrial & Engineering Chemistry Research*, 2009, **48**, 4300-4306.
48. R. Otomo, T. Yokoi, J. N. Kondo and T. Tatsumi, *Applied Catalysis A: General*, 2014, **470**, 318-326.
49. M. V. Opanasenko, W. J. Roth and J. Cejka, *Catalysis Science & Technology*, 2016, DOI: 10.1039/C5CY02079D.
50. E. Nikolla, Y. Román-Leshkov, M. Moliner and M. E. Davis, *ACS Catalysis*, 2011, **1**, 408-410.
51. R. Liu, J. Chen, X. Huang, L. Chen, L. Ma and X. Li, *Green Chemistry*, 2013, **15**, 2895-2903.
52. J. B. Joo, A. Vu, Q. Zhang, M. Dahl, M. Gu, F. Zaera and Y. Yin, *ChemSusChem*, 2013, **6**, 2001-2008.
53. Y. Shi, X. Li, J. Hu, J. Lu, Y. Ma, Y. Zhang and Y. Tang, *Journal of Materials Chemistry*, 2011, **21**, 16223-16230.

